CORROSION SCIENCE AND TECHNOLOGY, Vol.31, No.4(2002), pp.281~286

Influence of Iron-Silicon Ratio in Intermetallic Compound on Pitting Behavior of Aluminum

O.Seri and K.Furumata*

Department of Mechanical System Engineering, Muroran Institute of Technology
**Hakodate National College of Technology*

Iron and silicon elements are always observed in commercially pure aluminum. Some of them dissolve in aluminum matrix as solid solution, and others form the Al-Fe or Al-Fe-Si intermetallic compounds. The ratio of Fe/Si in the intermetallic compound phases is responsible for pitting attack behavior of the aluminum. In 1.0M NaCl solution not only aluminum but also iron in the intermetallic compound preferentially will dissolve. The higher Fe/Si ratio is, the easier dissolution of iron is. The preferential dissolution leads that solution surrounding the intermetallic compound particles will be changed to low pH due to the hydrolysis of aluminum and ferrous ions produced by the dissolution. The polarization measurements and metallurgical observations explain that the low pH will make the oxide film surround the particles weak or thin, and some of them provide a suitable concave for further propagation for the pitting attacks.

Keywords *: aluminum, pitting corrosion, iron, silicon, electrochemical measurement*

1. Introduction

From the environmental standpoint of sustainable developments for our global society, a concern has been raised about the recycle-use of industrial materials, especially aluminum and its alloys. For one reason, it is characteristically known that aluminum products can be easily recycled due to its rather low melting point among metals: aluminum recycled from scrap (secondary aluminum) requires much smaller energy consumption (about 6%) than when aluminum is extracted from bauxite (primary aluminum).[1] Aluminum is expected as one of the most recyclable materials, and at the same time aluminum should be obligated to be recycle-used.

When aluminum is recycle-used, the aluminum will be inevitably contaminated by some impurity elements such as iron and silicon. Metallurgy teaches that these elements form intermetallic second phases such as $FeAl_3$ or Al-Fe-Si ternary compounds in aluminum.[2] When these second phases are presented on the surface, the oxide film over them is thin or non-exist. The poor oxide film suffers from local attacks in an environment containing chloride ions. Understanding the corrosion behavior of the recycled-aluminum, which is usually contaminated by some impurity elements, is of considerable industrial significance. More-detailed researching the corrosion behavior of aluminum alloy 1100 will help the more fundamental understanding the corrosion behavior of recycled aluminum, because major alloy elements in aluminum alloy 1100 are same elements as ones in recycled-aluminum.

Many explanations have been proposed for the effect of the iron and silicon elements on corrosion behavior of aluminum.[3-6] It is well accepted that interface between the intermetallic phases and aluminum matrix has many defects in the oxide layer and provides the occurrences of pitting attacks. However, authors believe that their electrochemical mechanisms related to the defective oxide film layer could not be fully understood. There is one of the experimental facts that pitting attack density is extremely small compared to the surface density of intermetallic compound particles: the intermetallic particle density of aluminum containing 1% iron is roughly order of $10^{13}/m^2$, but the pitting attack density observed after corrosion is order of $10^3/m^2$.[6] There is far deference between them. Authors think that the existence of poor oxide film has only necessary conditions but not sufficient conditions in the process of pitting attack. The explanation may be not fully responsible for the strength of the oxide film structure. There will be another fundamental and reasonable electrochemical explanations for pitting attack progress.

2. Experimental

2.1 Specimens

The specimen 1100 used here is commercially pure aluminum 1100 plate, and specimen Al is 99.99% pure aluminum plate in Japanese market. The intermetallic compound specimen such as $FeAl_3$, α(Fe, Si) and β(Fe, Si) were made by casting a mixture of 99.99% aluminum, 99.9% iron and 99.9999% silicon. The $FeAl_3$ specimen was confirmed by X-ray diffraction analysis. The plate specimens of 15 mm wide, 80 mm long and 1 mm thick were prepared. Their surfaces were electronically masked with insulating tape, leaving uncovered area of 4.5 cm^2. The cast specimens have been first melted and then cast as rods of about 10 mm diameter, and their surfaces were electronically covered with the cured-epoxy resin, and one end of the rod was mechanically taper-polished, leaving uncovered area of about 1 cm^2. After decreasing by acetone, all specimens were pickled in a 10% NaOH solution at 353K for 60s. Rinsing with water, then specimens were pickled in a 30% HNO^3 solution at room temperature (about 298K) for 60s. To remove corrosion products adhered after corrosion test, specimens were dipped into a cleaning solution ($4\%Na_2CrO_4.4H_2O+10\%H_3PO_4$ aqueous solution) at 353K for 240s.

2.2 Solutions

An aqueous solution of 0.1 mole of NaCl (0.1M NaCl solution) was selected as test solution. Reagent grade NaCl, $AlCl_3.6H_2O$ and $FeCl_2.4H_2O$ were used. The volume of the test solution was one litter of de-ionized water. For measurement of anodic polarization curves, the oxygen free solution is obtained by continuous gas bubbling of high purity nitrogen gas ($99.999\%N_2$) through the solution. A moderated agitation by magnetic stirrer kept the solution fluidity uniform.

2.3 Measurements

The anodic and cathodic polarization curves have been potentiodynamically measured. The reference electrode is Ag/AgCl electrode in a saturated KCl solution. The electrode potentials of V vs. Ag/AgCl are quoted with respect to the Ag/AgCl reference electrode unless otherwise stated. The reference electrode was connected to the measuring cell with a salt bridge and Luggin capillary at the distance of 2 mm from the specimen. This distance makes iR drop negligibly small, then no correction to the polarization curves for iR drop was necessary. The platinum counter electrode and working electrode were placed in the same solution. When plotting the value of the corrosion potential~time, total measuring time of 600ks and its sampling intervals of 60s were selected. Scanning electron microscope (SEM) for surface observation of the specimen was routinely used. Electron probe micro analyzer (EPMA) was utilized for element analysis of the intermetallic compound phases: quantitative analysis of iron and silicon in compound particles, which are randomly selected, was carried out.

3. Results and disscussion

3.1 Corrosion potential~time curves

The variation of corrosion potential (E_{corr}) with time in 0.1M NaCl solution for a period of 600ks was measured. The result is shown in Fig.1.

During up to about 15ks immersion, the E_{corr} fluctuates between -617mV and -640mV, and for more than 15ks the E_{corr} decreases up-and-down with increasing time. At the immersion time of 600ks, its value shows approximately -680mV. It is roughly speaking that the E_{corr} of specimen 1100 corroded in 0.1M NaCl shifts gradually to less-noble potential with the time passing.

3.2 Observation of corroded surface

SEM surface observations of the specimen 1100 corroded in 3.1 were carried out at the immersion periods of 6ks (at early time of corrosion test) and 600ks (at the end of the corrosion test). They are shown in Fig. 2 (a)~Fig. 2 (f).

The Fig. 2(a) and Fig. 2(b) are the specimen surfaces before corrosion test as a blank test in different scales and places. The photograph of Fig. 2(b) is enlarged in order to show more detailed. Some white particles of intermetallic compound phases are observed. Fi. 2(c) and Fig. 2(d) show the surfaces of the specimen corroded at the period of 6ks. Pitting attack cavity of about 40

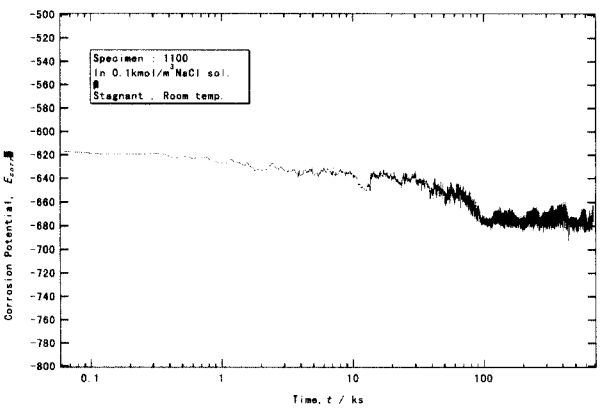

Fig. 1. Corrosion potential-time curve for 1100 aluminum in 0.1 $kmol/m^3$ NaCl solution.

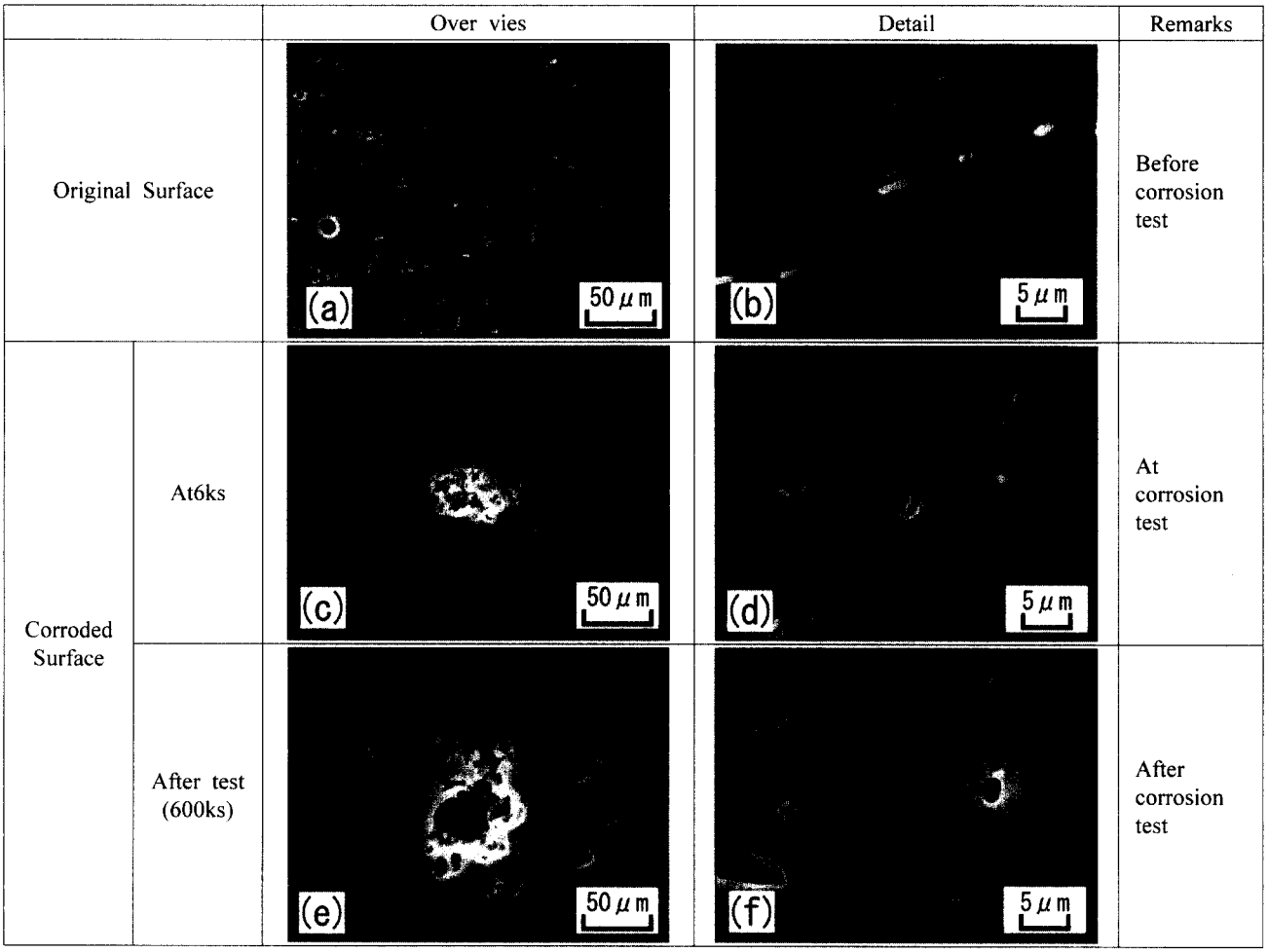

Fig. 2. Surface observations after 6ks (time=6ks) and 600ks (time=600ks) of corrosion test in 0.1 kmol/m^3 NaCl solution immersion including blank test.

micrometers in diameter is observed in the center of the Fig. 2(c). The characteristic concaves around the compound particles are observed in the center and at the upper right corner of the Fig. 2(d). Since these particles show slender and round shapes, they are named as "○-type particles" in this paper. On the other hand, the characteristic non-concave particles are observed at the left-hand side of the Fi. 2(d). Since these particles are unchanged and show the almost same shapes as Fig. (b), they are named as "□-type particles" in this paper. Fig. 2(e) and Fig. 2(f) show the surfaces of the specimen corroded at the period of 600ks. Pitting attack of 60 micrometer is observed in the center of the Fig. 2(e). The Fig. 2(f) is another corroded surface with free pitting attacks. It is noticed that the surface has less number of the compound particles compared to the original surface and shows a residual particle of □-type particle (left hand side).

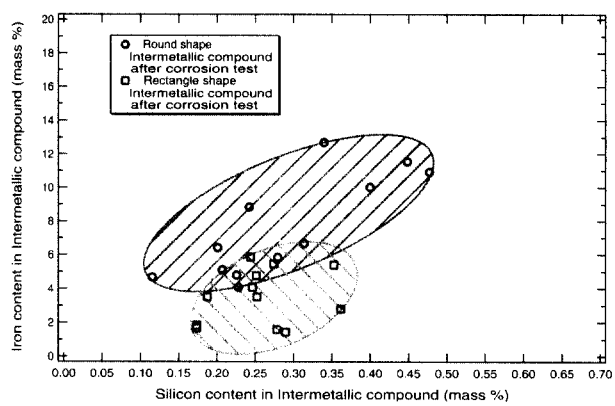

Fig. 3. Relationship between silicon and iron contents in residual intermetallic compound particles after corrosion test of Fig. 1.

3.3 EPMA analysis of intermetallic compound particles left

After corrosion test, EPMA analysis of iron and silicon

elements in twenty-four compound particles, which are selected at random, was carried out. Their results are summarized in Fig. 3.

The round mark and square mark correspond with the ○-type and the □-type intermetallic compound particles, respectively. Though the distribution of the ○-type and the □-type particles overlap partly, it will be generally accepted that the ○-type particles have larger iron content compared to the □-type particles.

3.4 Polarization curves

The polarization curve of specimen 1100 in deaerated 0.1M NaCl solution was measured. The result is shown in Fig. 4.

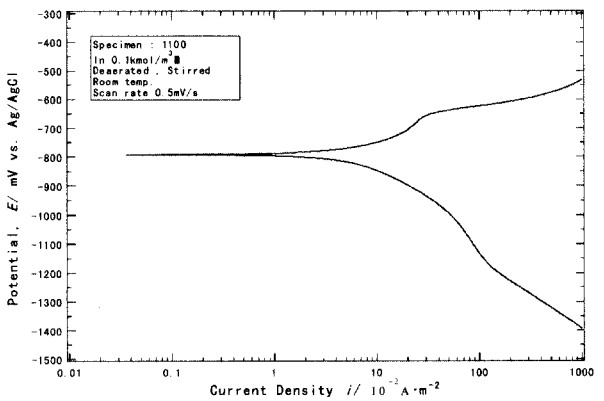

Fig. 4. Polarization curve of pure aluminum specimen (specimen 1100) in de-aerated 0.1M NaCl solution.

About -670mV of the pitting potential (E_{pit}), at which the anodic current density increases rapidly, is observed. The polarization curves of specimens $FeAl_3$, α(Fe, Si), β (Fe, Si) and Al in deaerated 0.1M NaCl solution were measured. They show that at around -660mV~ -680mV, the maximum peak anodic current densities are observed in all curves of the compound specimens. It is found that the higher content of iron in the compound is, the higher value of the maximum peak current density shows.[6)]

3.5 Cathodic polarization curves

The cathodic polarization curve of specimen 1100 in stagnant and open-to-air 0.1M NaCl solution was measured. The result shows that the plateau of cathodic current density (i_L), which is a sign of the limiting cathodic current density for dissolved oxygen reduction reaction, is observed at -650 mV~-1050 mV. The cathodic polarization curves of specimen $FeAl_3$, α(Fe, Si) and β (Fe, Si) in stagnant and open-to-air 0.1M NaCl solution were measured. Their results are shown in Fig. 5. Plateaus of the i_L appear in all of the curves. The value of i_L is related to the iron content in the compound phases: the higher content of iron in the compound specimen is, the larger value of the iL shows.[6)]

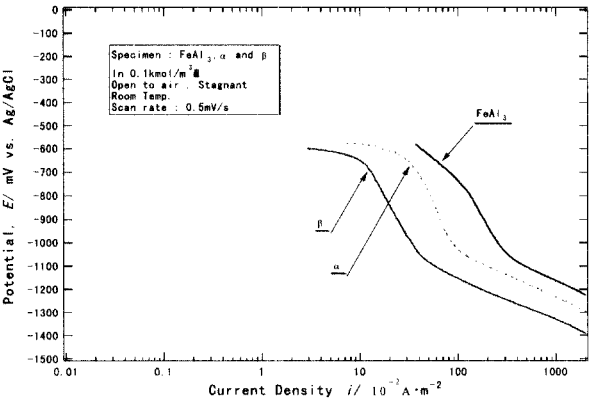

Fig. 5. Cathodic polarization curves of intermetallic compound specimens(specimen $FeAl_3$, α and β) in stagnant 0.1 kmol/m^3 NaCl solution.

3.6 Polarization curves in a mixture solution of NaCl and $AlCl_3$

The polarization curves of specimen $FeAl_3$, α(Fe, Si), β(Fe, Si) and Al in deaerated 0.1M NaCl + xM $AlCl_3$ (x=0.1 M and 1.0M) solutions were measured. The results of x=0.1M NaCl (0.1M NaCl + 0.1M AlC_3 solution) is shown in Fig. 6.

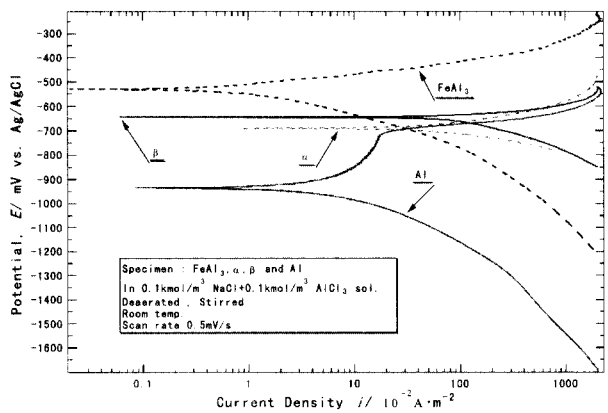

Fig. 6. Polarization curves of intermetallic specimens (specimen $FeAl_3$, α and β) and pure aluminum specimen (specimen Al) in de-aerated 0.1M NaCl + 0.1M $AlCl_3$ solution.

The value of the E_{pit} for specimen Al is -715mV. The anodic polarization resistances of compound specimens for specimen $FeAl_3$, α(Fe, Si) and β(Fe, Si) decrease when the $AlCl_3$ is added to the NaCl solution. The anodic polarization resistances of compound specimens also decrease with increase of $AlCl_3$ concentration.

When considering the electrochemical behavior of iron in compound phases, it is necessary to focus on the dissolution reaction of the $FeAl_3$ phase. The potential-pH diagram of $FeAl_3$ compound indicates that the stable chemical forms of $FeAl_3$ are ferrous ions and aluminum hydroxide at the electrochemical conditions (potential of -617mV and solution pH of 6, which are in Fig. 1).[12] The simultaneous dissolution of the $FeAl_3$ phase may occur and then will be described by following,

$$FeAl_3 + 9H_2O = Fe^{2+} + 3Al(OH)_3 + 9H^+ + 11e \quad (1)$$

$$E_{eq}(FeAl_3/Fe^{2+}, Al(OH)_3) = -1.25 - 0.048pH + 0.005\log a_{Fe^{2+}}$$

where, E_{eq} $(FeAl_3/Fe^{2+},Al(OH)_3)$ is the equilibrium potential among $FeAl_3$, ferrous ions and aluminum hydroxide (V vs.SHE). $a_{Fe^{2+}}$ is activity of ferrous ions.

During the propagation of pitting attack, it is necessary to consider the change of the electrochemical conditions. The conditions in the pitting cavities have been changed for the long period of immersion. They are potential of -680mV from Fig. 1 and will be the supposed pH value of about 2~4[8] in a pitting cavity. The stable chemical forms will be ferrous ions and aluminum ions. The simultaneous dissolution of the $FeAl_3$ phase may occur and be described by following,

$$FeAl_3 = Fe^{2+} + 3Al^{3+} + 11e \quad (2)$$

$$E_{eq}(FeAl_3/Fe^{2+}, Al^{3+}) = -1.39 + 0.005\log\{ a_{Fe^{2+}} \cdot a_{Al^{3+}} \}$$

where, $E_{eq}(FeAl_3/Fe^{2+}, Al^{3+})$ is the equilibrium potential among $FeAl_3$, ferrous ions and aluminum ions (V vs.SHE). $a_{Al^{3+}}$ is activity of aluminum ions.

It is understood that the reaction of eq.(1) will be influenced by the accompanied cathodic reaction of oxygen reduction reaction. Namely the dissolution rate of the eq.(1) will decrease, due to alkalizing occurred on the $FeAl_3$ particles and to the slow solid~solid reaction. Authors think that the eq.(1) practically may not well-work in the ordinary corrosion process.

The reaction of eq.(2) will take important part in the propagation of pitting attacks.[13] The $FeAl_3$ particle in active pitting cavities, which provide the environments of high concentration of hydrogen ions and chloride ions, will vigorously be dissolved into ferrous ions and aluminum ions. Anodic polarization measurements show that simultaneous dissolution of eq.(2) will easily occur in the NaCl + $AlCl_3$ solution, due to small anodic polarization resistance.

In order to understand the pitting corrosion of the specimen 1100 corroded in 0.1M NaCl solution, it is convenient to classify its corrosion process into two steps: pitting initiation process (-617mV > E_{corr} > -680mV, or immersion period < 105ks) and pitting propagation process (E_{corr} < -680mV, or immersion period > 105ks)

(Pitting initiation process)

As the start of pitting attack, it is well accepted that the cathodic reaction is oxygen reduction reaction, which may occur on the iron-rich compound particles such as FeAl3 phase. Anodic reaction is dissolution reaction, which occurs at the weak interfaces between aluminum matrix and compound particles. Their reactions are as follows,

$$O_2 + 2H_2O + 4e = 4OH^- \quad (3)$$

$$Al + 3H_2O = Al(OH)_3 + 3H^+ + 3e \quad (4)$$

In order to understand the relation between eq.(3) and eq.(4), the anodic polarization curve of specimen Al shown and cathodic polarization curves of specimen $FeAl_3$, α (Fe, Si) and β (Fe, Si) are superimposed. It clearly indicates that reduction reaction of dissolved oxygen increases with iron-rich content in the compound. This suggests that aluminum matrix surrounded by higher iron content compounds will be easily dissolved. The eq.(4) suggests that the active anodic site will be covered with corrosion product of $Al(OH)_3$, which has good adhesion ability and pH buffer characteristics. The eq.(4) also suggested that the atmosphere of the anodic site will become acidic. These provide suitable conditions for occurrence of embryos for pitting attacks. The electrochemical conditions probably depend on the complex combinations between environments such as flow pattern, flow velocity and compound phases such as particles' largeness, distribution and the characteristics. When the aluminum matrix around the particles is dug up by general dissolution, then the particles, which often show round shape (○-type particles), will easily drop away (Fig. 2(d)).

(Pitting propagation process)

In the pitting growth process, the anodic reactions are dissolution reactions of both aluminum matrix and compound particles in the pitting cavities. The cathodic reaction in the pitting cavities is hydrogen evolution reaction occurred on the newly exposure surface of the compound particles or on the deposited iron, which is produced by reduction of ferrous ions, underneath the pitting cavity.[14] Their reactions are followings:

$$Al = Al^{3+} + 3e \quad (5)$$

$$2H^+ + 2e = H_2 \quad (6)$$

The surface morphology at pitting potential region is

characteristically crystallographic facet appearances. They are shown in Fig. 2(e) and Fig. 12(d). It is often observed that the crystallographic facet will change to dimple facet from crystallographic facet, due to the edge dissolution by low pH atmosphere in active pitting cavity.[15)]

4. Conclusion

The corrosion behavior of industrial pure aluminum 1100, which is corroded in aerated and stirred 0.1M NaCl solution for the period of 600ks, was observed from the points of surface observations, EPMA analysis and electrochemical measurements. The pitting attacks initiate the boundary between aluminum matrix and intermetallic compound particles containing higher iron. Almost all of the intermetallic particles may disappear by the simultaneous dissolution of iron and aluminum in the compound phase and by the dropping of the interface. When a few suitable environments for the further pitting propagation, which provide the corrosion product forming, chloride ion enrichment and hydrogen ion entrance, the pit cavities will become active and enlarge with an appearance of crystallographic or dimple facet.

References

1. T. E. Graedel and B. R. Allenby, Industrial Ecology, Prentice Hall, pp.195-196 (1995).
2. ASM International, Metals Handbook Ninth Edition, Volume 13 Corrosion pp.583-609 (1987).
3. G. Wranglen, An Introduction to Corrosion and Protection of Metals, Chapman and Hall, pp.94-98 (1985).
4. J. R. Paris, Corrosion of Aluminum and Aluminum Alloys, ASM International, pp.33-35 (1999).
5. G. Itoh, Fusyokukagaku to bousyokugijyutu, Corona-Shya, pp.207-208 (1971).
6. O. Seri and N. Masuko, *Journal of Japan Institute of Light Metals*, **35**, 98 (1985).
7. O. Seri and K. Tagashira, *Corrosion Science*, **30**, 87 (1990).
8. O. Seri and K.Tagashira, *Journal of Japan Institute of Light Metals*, **38**, 191 (1988).
9. O. Seri and M.Imaizumi, *Corrosion Science*, **30**, 1121 (1990).
10. L. F. Mondolfo, Aluminum Alloys, Butterworth, O.K., pp.534-537 (1976).
11. M. Pourbaix, Atlas of Electrochemical Equilibria, Pergamon Press, pp.458-463 (1966).
12. O. Seri, *J. Japan Inst. Metals*, **62**, 167 (1998).
13. O. Seri and N.Masuko, *Journal of Japan Institute of Light Metals*, **34**, 41 (1984).
14. O. Seri, *Corrosion Science*, **36**, 1789 (1994).
15. K. Tohma and Y. Takeuchi, *Journal of Japan Institute of Light Metals*, **31**, 422 (1980).